

A Laboratory Investigation on Thermal Properties of the Opalinus Claystone

M. Monfared · J. Sulem · P. Delage ·
M. Mohajerani

Received: 18 March 2011 / Accepted: 25 July 2011 / Published online: 23 August 2011
© Springer-Verlag 2011

Abstract Some aspects of the thermal behavior of the Opalinus claystone are investigated through laboratory tests conducted on a new hollow cylinder triaxial apparatus specially designed for studying the thermo-hydro-mechanical behavior of very low permeable materials. Two hollow cylinder samples are first resaturated under isotropic stress state equal to the mean effective in situ one in order to minimize swelling and induced damage during the resaturation phase. Two drained heating–cooling cycles are performed on the first sample of Opalinus claystone. During the first cycle, a thermo-elasto-plastic response similar to that of plastic clays with low overconsolidation ratio is obtained. The thermal hardening of the sample is demonstrated by the quasi-reversible behavior of the sample during the second heating–cooling cycle. An undrained heating test performed on the second sample of Opalinus claystone induces an excess pore pressure in this sample. This induced pore pressure is attributed to the higher thermal expansion coefficient of pore water compared to that of the solid phase. It is shown that the excess pore pressure generated in the sample by undrained heating cannot be modeled by considering the free water thermal expansion coefficient. The thermal expansion coefficient of the Opalinus claystone water is back-analyzed from the

experimental results which show a higher value than free water.

Keywords Opalinus claystone · Thermal properties · Saturation · Drained test · Undrained test

1 Introduction

The storage of long life high activity radioactive waste in deep geological formations appears to be an interesting solution for a long-term repository. In this regard, storage in low permeability claystones with favorable self sealing properties (Bastiaens et al. 2007) is considered as an appropriate option in various countries including Switzerland (Opalinus claystone; Thury and Bossart 1999) and France (Callovo-Oxfordian mudstone; ANDRA 2005). The heat emitted by high-level radioactive waste increases temperature around the galleries whereas the maximum admissible temperature in the Swiss repository design is 90°C (Nagra 2002b). Elevated temperature can induce irreversible deformation and thermal excess pore pressure in the near field. This latter leads to thermo-mechanical failure (Hueckel and Pellegrini 1991) or to the reactivation of existing fractures (Monfared et al. 2011b) in host rocks. The transport properties of the geological barrier can be hence modified, affecting the tightness and long-term safety of the storage. Therefore, the coupling between thermal phenomena and the response of the claystone must be further investigated. In situ investigations have been performed on the thermal properties of the Opalinus claystone in the Mont-Terri Underground Research Laboratory, (Hohner and Bossart 1998; Mügler et al. 2006; Jobmann and Polster 2007; Kull et al. 2007; Gens et al. 2007). Most of laboratory works on the thermal response of Opalinus

M. Monfared (✉) · J. Sulem · P. Delage · M. Mohajerani
Université Paris-Est, UR Navier, CERMES,
Ecole des Ponts ParisTech, 6-8 av. Blaise Pascal,
77455 Marne-la-Vallée Cedex 2, France
e-mail: monfared@cermes.enpc.fr

Present Address:
M. Monfared
Soil Mechanics Laboratory,
Ecole Polytechnique Fédérale de Lausanne (EPFL),
Lausanne, Switzerland

claystone have been performed in unsaturated condition (Jobmann and Polster 2007; Zhang et al. 2007). Therefore, further investigation for fully saturated samples is still needed.

When testing low permeability materials extremely slow loading or heating rates must be used in order to avoid possible pore fluid overpressure (in drained tests) and possible heterogeneity of the pore pressure (in undrained tests) inside the sample. In this paper, the thermo-mechanical behavior of Opalinus claystone is experimentally investigated by means of a new hollow cylinder triaxial apparatus with a short drainage path specially designed for very low permeability materials (Monfared et al. 2011a). The investigation carried out concerns both the drained and undrained response of Opalinus claystone, with a special emphasis put on thermal pore fluid pressurization.

2 Thermo-Poro-Elasticity Background

The theoretical framework of thermo-poro-elasticity used to analyze the experimental data is briefly recalled in the following. Basic principles have been presented in various earlier studies (Coussy 2004; McTigue 1986; Rice 2006; Ghabezloo et al. 2009).

In the following, compression strain is considered positive as conventionally adopted in soil mechanics ($\varepsilon_V = -\frac{dV}{V}$). To describe the sample volume change (dV) and the pore volume change (dV_ϕ), the Terzaghi effective stress ($p' = p - u$), the pore pressure (u) and the temperature (T) are chosen as independent variables:

$$\frac{dV}{V} = -c_d dp' - c_s du + \alpha_d dT \quad (1)$$

$$\frac{dV_\phi}{V_\phi} = -\frac{c_d - c_s}{\phi} dp' - c_\phi du + \alpha_\phi dT \quad (2)$$

where $\phi = \frac{V_\phi}{V}$ is the Eulerian porosity and c_d , c_s and c_ϕ are the drained, solid and pore volume compressibility, respectively, which are defined as follows:

$$c_d = -\frac{1}{V} \left(\frac{\partial V}{\partial p'} \right)_{u,T}, \quad c_s = -\frac{1}{V} \left(\frac{\partial V}{\partial u} \right)_{p',T},$$

$$c_\phi = -\frac{1}{V_\phi} \left(\frac{\partial V_\phi}{\partial u} \right)_{p',T} \quad (3)$$

α_d and α_ϕ are the drained and the pore volume thermal expansion coefficient, respectively:

$$\alpha_d = \frac{1}{V} \left(\frac{\partial V}{\partial T} \right)_{u,p'}, \quad \alpha_\phi = \frac{1}{V_\phi} \left(\frac{\partial V_\phi}{\partial T} \right)_{u,p'} \quad (4)$$

The experimental measurement of parameters c_ϕ and α_ϕ is difficult and they will be assumed here equal to the solid phase compressibility (c_s) and solid phase thermal expansion (α_s).

For a saturated material, the fluid mass inside the representative elementary volume is:

$$M_w = \phi \rho_w V \quad (5)$$

where ρ_w is the water unit mass.

Derivation of Eq. 5 gives:

$$dM_w = \phi \rho_w V \left(\frac{d\phi}{\phi} + \frac{d\rho_w}{\rho_w} + \frac{dV}{V} \right) \quad (6)$$

From the definition of the porosity one can write:

$$\frac{d\phi}{\phi} = \frac{dV_\phi}{V_\phi} - \frac{dV}{V} \quad (7)$$

the change in water unit mass by pressure and temperature is obtained by:

$$\frac{d\rho_w}{\rho_w} = c_w du - \alpha_w dT \quad (8)$$

where c_w is the water compressibility and α_w is the water thermal expansion coefficient.

Introducing Eqs. 8 and 7 into Eq. 6 gives:

$$dM_w = \phi \rho_w V \left(-\frac{c_d - c_s}{\phi} d\sigma + \frac{S}{\phi} du - (\alpha_w - \alpha_s) dT \right) \quad (9)$$

where S is the storage coefficient:

$$S = c_d - c_s + \phi(c_w - c_s) \quad (10)$$

During an undrained thermal test at constant total stress the thermally induced excess pore pressure is obtained by setting $dM_w = 0$ in Eq. 9:

$$du = \Lambda dT \quad (11)$$

where Λ is the thermal pressurization coefficient:

$$\Lambda = \frac{\phi(\alpha_w - \alpha_s)}{S} \quad (12)$$

The corresponding volumetric deformation can be obtained from Eq. 1:

$$\frac{dV}{V} = \alpha_u dT \quad (13)$$

where α_u is the undrained thermal expansion coefficient:

$$\alpha_u = \alpha_d + \Lambda(c_d - c_s). \quad (14)$$

3 Material and Methods

3.1 Opalinus Claystone

Tests have been performed on specimens of Opalinus claystone extracted parallel to the bedding in 106 mm diameter cores from the Underground Research Laboratory of Mont-Terri in Switzerland. The total claystone porosity

deduced from oven drying at 105°C during 24 h is around 18% whereas the mercury intruded porosity measured by Muñoz (2006) at a maximum pressure of 219 MPa is between 9 and 11%.

The Opalinus claystone from shaly facies is composed of approximately 65% clay minerals [Illite (17%), illite-smectite mixed layer (10%), chlorite (8%) and Kaolinite (30%)] and 35% of non clayey minerals composed of 20% quartz, 11% carbonate (8% calcite, 1% Dolomite/ankerite, 2% Siderite), 2.5% framework silicate (albites, K-feldspar) and small amount of pyrite (1%) and organic carbon (0.5%) (Mazurek 1999; Bossart et al. 2002; ANDRA 2005).

3.2 Testing Device

Tests have been performed in a new hollow cylinder triaxial cell with a short drainage path specially designed to study the thermo-hydro-mechanical behavior of low permeability materials (Fig. 1a). The details of the cell are presented in Monfared et al. (2011a). Hollow cylinder samples have an internal diameter $\varphi_{\text{int}} = 60$ mm, an external diameter $\varphi_{\text{ext}} = 100$ mm and a height $H = 70\text{--}80$ mm. Standard triaxial stress conditions are achieved by applying the same confining pressure in both the inner and outer cylindrical faces of the sample. As shown in Fig. 1a and b, a major advantage of this device is the enhanced drainage allowed by the geotextiles placed along the internal and external walls of the hollow cylinder sample. Geotextile bands have a height between $H/2$ and $H/3$ and are placed in the middle height of the sample. The drainage path is hence reduced to

half the thickness of the sample (10 mm). In such conditions, Monfared et al. (2011a) showed that the time needed to resaturate an initially unsaturated Opalinus claystone sample is reduced by a factor seven compared to standard full cylinder triaxial specimen with drainage at top and bottom. The short drainage path also permits to satisfactorily achieve fully drained conditions, i.e. negligible induced excess pore pressure, during mechanical and thermal loading with faster loading rates. Another interesting feature is the possibility to perform radial permeability tests and to directly capture the effect of shear bands formed during deviatoric loading that can be a preferential hydraulic path for radial flow.

This cell is equipped with a local strain measurement system with two axial and four radial local strain transducers (LVDT). Figure 1b shows a schematic view of the hydraulic connections between the sample, the pressure–volume controllers (PVC) and the pressure transducers (PT). The system includes a high pressure (10 MPa) pressure–volume controller (PVC1) to apply the confining pressure in the inner and outer cell volumes. Three PVCs are used to apply and control the pore fluid pressure: PVC2 is connected to the upper and lower ends of the sample, PVC3 to the inner boundary and PVC4 to the outer boundary. The cell is also equipped with a resistive heating belt around the cell connected to a temperature regulator that ensures a precision of $\pm 0.1^\circ\text{C}$. Temperature is measured inside the cell close to the sample by a thermocouple. An insulating cover is put around the cell in order to limit heat exchanges with the environment.

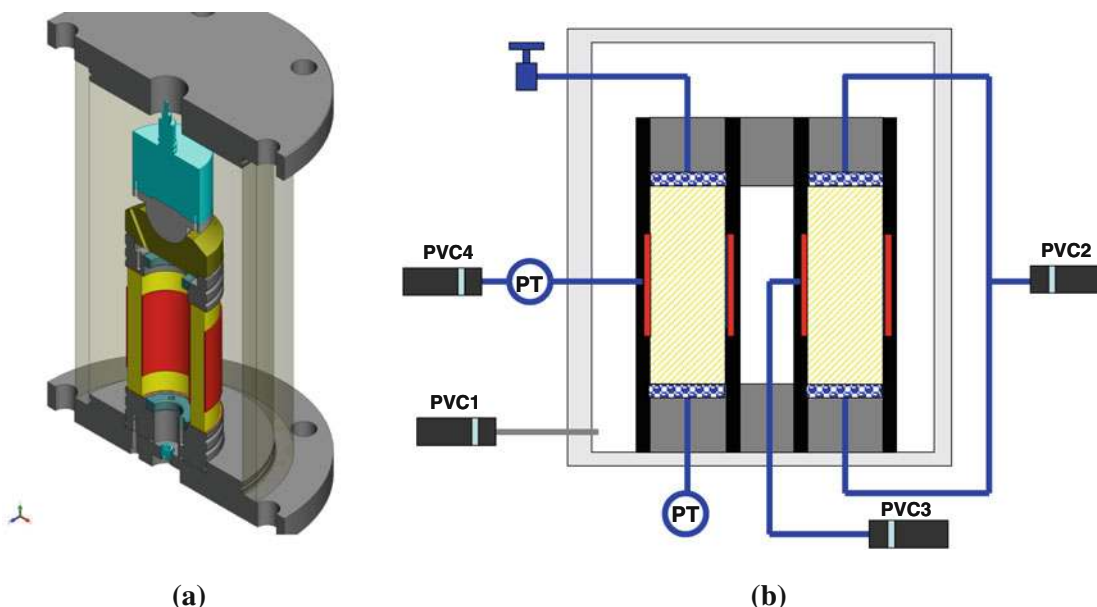


Fig. 1 a Hollow cylinder triaxial cell with a short drainage path, b general setting of the hydraulic connections

3.3 Effect of the Drainage System on the Measured Undrained Parameters

Undrained conditions are applied in the laboratory tests by closing the valves at the extremity of the drainage system. Due to the compressibility and to the thermal expansion of the fluid and of the drainage system, there is some fluid exchange between the sample and the drainage system that alters the undrained condition ($dM_w = 0$). Consequently, the measured pore pressure is affected by the compressibility and the thermal expansion of the drainage system. A correction accounting for these effects was presented by Bishop (1976), with an extension to temperature effects recently proposed by Ghabezloo and Sulem (2010). A detailed analysis of the effect of the drainage system on the undrained mechanical properties evaluated in the hollow cylinder triaxial cell is presented in Monfared et al. (2011a). In this analysis, the compressibility of the porous elements around the sample is taken into account to have a more precise correction method rather than that presented by Bishop (1976) and Ghabezloo and Sulem (2010). The analysis is extended here to the effects of temperature.

The sample, the porous elements (porous disks and geotextiles) and the connecting lines are submitted to a temperature change ΔT and a pore pressure change Δu . The method presented by Bishop (1976) is used to decompose the problem into independent sub-problems as presented in Fig. 2.

The volume change of each element is written in Table 1. In this table, V_L and c_L are the volume and the compressibility of the connecting lines (including the pore pressure transducers), ϕ_e and V_e are the porosity and the volume of the porous element, c_{se} and c_{de} are the solid phase compressibility and the drained compressibility of the porous element, α_{se} and α_L are the thermal expansion coefficients of the porous element and of the connecting lines, respectively. The temperature change along the connecting lines is not homogenous because one part of the connecting lines is situated inside the cell, at the same temperature as the sample whereas another part is situated outside the cell at room temperature. Following Ghabezloo

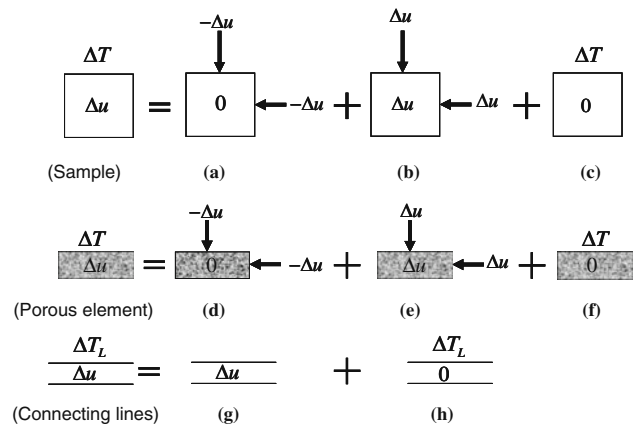


Fig. 2 Decomposition of the testing system into a porous sample, a porous element and connecting lines

homogeneous temperature field. ΔT_L is defined by a parameter β equal to the ratio between the temperature change of the sample ΔT and the equivalent temperature change of the connecting lines ΔT_L :

$$\Delta T_L = \beta \Delta T \quad (15)$$

In undrained condition, the overall volume change of the system (column 4 of Table 1) is equal to the sum of the volume change of its constituents (columns 2 and 3 of Table 1). After some algebra, the following relation is obtained between the measured thermal pressurization coefficient and the parameters of the system:

$$\begin{aligned} \Lambda^{\text{mes}} &= \frac{\Delta u}{\Delta T} \\ &= \frac{\phi(\alpha_w - \alpha_s) + \frac{V_e}{V} \phi_e (\alpha_w - \alpha_{se}) + \frac{V_L}{V} \beta (\alpha_w - \alpha_L)}{S + \frac{V_e}{V} S_e + \frac{V_L}{V} (c_L + c_w)} \end{aligned} \quad (16)$$

where S_e is the storage coefficient of the porous element:

$$S_e = c_{de} + \phi_e c_w \quad (17)$$

Comparing Eqs. 12 and 16, the following form can be presented for the corrected (true) thermal pressurization coefficient:

$$\Lambda^{\text{cor}} = \frac{\phi(\alpha_w - \alpha_s)}{S} = \frac{\Lambda^{\text{mes}}}{1 + \frac{1}{\phi V (\alpha_w - \alpha_s)} [\phi_e V_e (\alpha_w - \alpha_{se}) + \beta V_L (\alpha_w - \alpha_L) - \Lambda^{\text{mes}} (V_e S_e + V_L (c_w + c_L))]} \quad (18)$$

and Sulem (2010), an equivalent temperature change (ΔT_L) is introduced in such a way that the volume change of the connecting lines under a homogeneous temperature change equal to ΔT_L is the same as that induced by the real non-

By considering the volumetric response of the sample, the effect of porous disk and geotextile can be superposed, Eq. 18 can be rewritten as: where subscripts p and g concern the porous disk and the geotextile properties,

$$\Lambda^{cor} = \frac{\Lambda^{mes}}{1 + \frac{1}{\phi V(\alpha_w - \alpha_s)} [\phi_p V_p(\alpha_w - \alpha_{sp}) + \phi_g V_g(\alpha_w - \alpha_{sg}) + \beta V_L(\alpha_w - \alpha_L) - \Lambda^{mes}(V_p S_p + V_g S_g + V_L(c_w + c_L))]} \tag{19}$$

respectively. Once the thermal pressurization coefficient is corrected, the measured undrained thermal expansion coefficient (α_u^{mes}) can also be corrected from the effect of the drainage system. By considering Eq. 14 and using the following relationship between the measured thermal pressurization coefficient (Λ^{mes}) and the measured undrained thermal expansion coefficient (α_u^{mes}):

$$\alpha_u^{mes} = \alpha_d + \Lambda^{mes}(c_d - c_s) \tag{20}$$

the following expression is obtained for the corrected undrained thermal expansion coefficient:

$$\alpha_u^{cor} = \alpha_u^{mes} - (\Lambda^{mes} - \Lambda^{cor})(c_d - c_s) \tag{21}$$

The volumes of the different components of the drainage system are given in Table 2.

The drained compressibility of the porous disk and the geotextile are equal to $c_{dp} = 1.02 \text{ GPa}^{-1}$ and $c_{dg} = 9.33 \text{ GPa}^{-1}$, respectively. The compressibility of the connecting lines (c_L) is 0.32 GPa^{-1} (Monfared et al. 2011a). To correct the effect of the drainage system during the undrained thermal tests, the parameters β and α_L should be experimentally determined. To do so, an undrained heating test is performed on a metallic sample. In this test, temperature is increased from 27 to 45°C and the induced pore pressure in the bottom drainage of the sample is monitored by a pressure transducer (Fig. 1b). The induced pore pressure can be modeled by considering a zero porosity and zero storage coefficient ($S = 0$) in the metallic sample in Eq. 16 and neglecting the solid phase compressibility of the porous disk, which gives:

$$\Delta u = \frac{V_p \phi_p (\alpha_w - \alpha_{sp}) + V_L \beta (\alpha_w - \alpha_L)}{V_p (c_{dp} + \phi_p c_w) + V_L (c_L + c_w)} \Delta T \tag{22}$$

The volume of the porous disk and connected line are 10,053 and 11,722 mm³, respectively (Table 2). The porosity of the stainless steel porous disk (ϕ_p) is 0.22 and its thermal expansion coefficient (α_{sp}) is $5.2 \times 10^{-5}/^\circ\text{C}$. By considering the change of water thermal expansion coefficient (α_w) and water compressibility (c_w) with temperature (Spang 2002) and considering $\beta = 0.6$ and $\alpha_L = 2 \times 10^{-4}/^\circ\text{C}$, the estimated induced pore pressure from Eq. 22 is in very good agreement with the experimental data, as shown in Fig. 3.

Considering the thermal expansion coefficient of the geotextile $\alpha_{sg} = 2.3 \times 10^{-4}/^\circ\text{C}$, Eqs. 19 and 21 can now be used to correct the measured thermal pressurization coefficient (Λ^{mes}) and the measured undrained thermal expansion coefficient (α_u^{mes}) during an undrained thermal test.

3.4 Testing Program

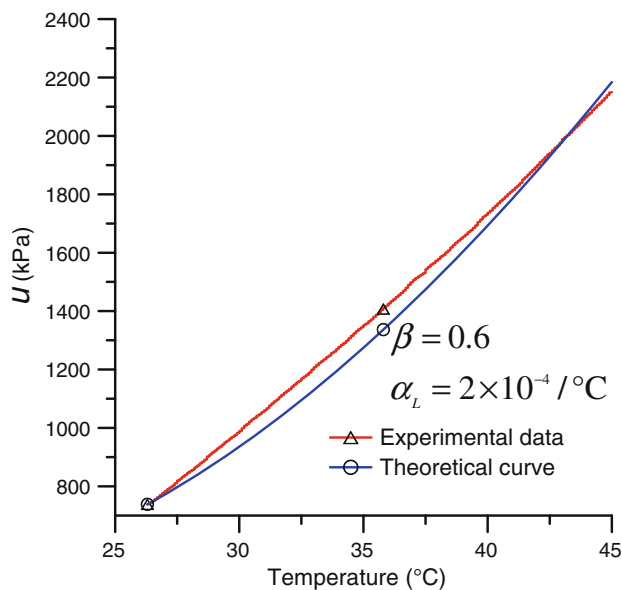
To prepare a hollow cylinder sample, the 106 mm diameter cylindrical core (slightly larger than the required 100 mm external diameter) is carefully cut at the desired length (around 72 mm) by using a hand saw. The cylinder is covered by a neoprene membrane to prevent drying and placed in a special metal mould of the same diameter in which it is firmly held. The inner hole of the sample is then cored in dry conditions by using a diamond coring bit of 60 mm diameter. Two hollow cylinder samples (TO1 and TO2) have been prepared. Both samples have been cored parallel to bedding planes because of the technical difficulty of preparing Opalinus samples with bedding planes perpendicular to the sample axis without dinking.

Table 1 Variations of volume of the sample, porous element, their constituents and the connecting lines for the independent problems presented in Fig. 2

	Volume change of constituents		Volume change of element
	Solid phase	Pore fluid phase	
(a) Sample	$Vc_s \Delta u$	0	$Vc_d \Delta u$
(b) Sample	$-(1 - \phi)Vc_s \Delta u$	$-\phi Vc_w \Delta u$	$-Vc_s \Delta u$
(c) Sample	$(1 - \phi)V\alpha_s \Delta T$	$\phi V\alpha_w \Delta T$	$V\alpha_s \Delta T$
(d) Porous element	$V_e c_{se} \Delta u$	0	$V_e c_{de} \Delta u$
(e) Porous element	$-(1 - \phi_e)V_e c_{se} \Delta u$	$-\phi_e V_e c_w \Delta u$	$-V_e c_{se} \Delta u$
(f) Porous element	$(1 - \phi_e)V_e \alpha_{se} \Delta T$	$\phi_e V_e \alpha_w \Delta T$	$V_e \alpha_{se} \Delta T$
(g) Connecting lines		$-V_L c_w \Delta u$	$V_L c_L \Delta u$
(h) Connecting lines		$V_L \alpha_w \Delta T_L$	$V_L \alpha_L \Delta T_L$

Table 2 Volume of the porous elements and connecting lines

Drainage	V_{drainage} (mm^3)	$V_{\text{porous element}}$ (mm^3)	ϕ	$V_{\text{connecting line}}$ (mm^3)
Lower (metallic)	13,934	10,053	0.22	11,722
Upper (metallic)	8,975	10,053		6,763
Outer (geotextile)	7,100	5,654	0.3	5,403
Inner (geotextile)	3,500	4,241		2,228

**Fig. 3** Calibration test on a metallic sample for the effect of thermal expansion of the drainage system during undrained heating: Induced pore pressure in the bottom drainage by the temperature change

The drained thermal behavior of Opalinus claystone is investigated on specimen TO1 by running two drained heating–cooling cycles between 25 and 80°C. The undrained behavior is investigated on specimen TO2 through an undrained heating test from 25 to 55°C. Both tests were run under a mean total stress and initial back pressure equal to the in situ ones (4.1 and 2.2 MPa, respectively) (Martin and Lanyon 2003).

3.5 Resaturation Process

The initial water content of the sample is 6.5%, which is smaller than the saturated water content for this clay stone (8.7%, after Muñoz 2006). In order to minimize any swelling-induced damage (Mohajerani et al. 2011), sample resaturation should be performed under in situ effective stress (Delage et al. 2007). The in situ stress in the Mont-Terri Underground Laboratory is highly anisotropic with ($\sigma_1 = 6\text{--}7$ MPa, $\sigma_2 = 4\text{--}5$ MPa, $\sigma_3 = 0.6\text{--}2$ MPa after Martin and Lanyon 2003). It is obvious that such a complex anisotropic stress state can not be applied in a triaxial cell, this is why the resaturation process is performed under an isotropic stress equal to the in

situ total mean stress (4.1 MPa) and a back pressure equal to in situ pore pressure (2.2 MPa) applied through the four drainage connections. Figure 4a shows the water intake by the sample during resaturation phase measured by the pressure-volume controllers as well as the sample volumetric strain deduced from the response of the LVDT transducers. Both curves exhibit a bi-linear response with a steep slope during the first 12 h. As shown in Monfared et al. 2011a, this section is related to the pore pressure diffusion inside the sample, up to reaching positive values in all points of the sample. The second part with a gentler slope indicates a continuous sample swelling and may be related to (i) the isotropic stress applied that is not exactly similar to the anisotropic in-situ stress conditions and (ii) some enhanced swelling capacity linked to some damage induced in the sample prior to testing, as shown by Mohajerani et al. 2011. After 132 h, the Skempton coefficient is measured by running an undrained isotropic compression test in which the pressure change is monitored by the pressure transducers connected at the bottom and at the external wall of the sample. Figure 4b shows the response of the pressure transducers for a confining pressure increase of 500 kPa. The responses of both transducers are similar, showing the homogeneity of the pore pressure field in the sample. The measured Skempton coefficient (slope of the pore pressure vs. confining pressure curve in Fig. 4b) is equal to 0.93. Once corrected from the effects of the drainage system (Monfared et al. 2011a), a value of 0.95 is obtained.

This value can be compared with the theoretical expression of the Skempton coefficient for a saturated elastic material, given by:

$$B = \frac{c_d - c_s}{c_d - c_s + \phi(c_w - c_s)}. \quad (23)$$

With a drained compressibility (c_d) taken equal to $1.85 \times 10^{-6} \text{ kPa}^{-1}$ (Sect. 4.2.2), the solid phase compressibility equal to $2 \times 10^{-8} \text{ kPa}^{-1}$ (Monfared et al. 2011a), the water compressibility (c_w) equal to $4.49 \times 10^{-7} \text{ kPa}^{-1}$ and the porosity equal to 0.18, the theoretical value for B is 0.96, which is quite close to the experimental one (0.95), confirming that excellent sample saturation can be achieved in very low permeability materials within a reasonable period of time thanks to the short drainage path that characterizes the hollow cylinder triaxial device.

4 Experimental Results

4.1 Drained Thermal Heating

The drained thermal behavior of the Opalinus claystone is investigated on sample TO1 by performing two heating–cooling cycles from 25 to 80°C. To ensure drained conditions, all the four drainage connections (top, bottom and

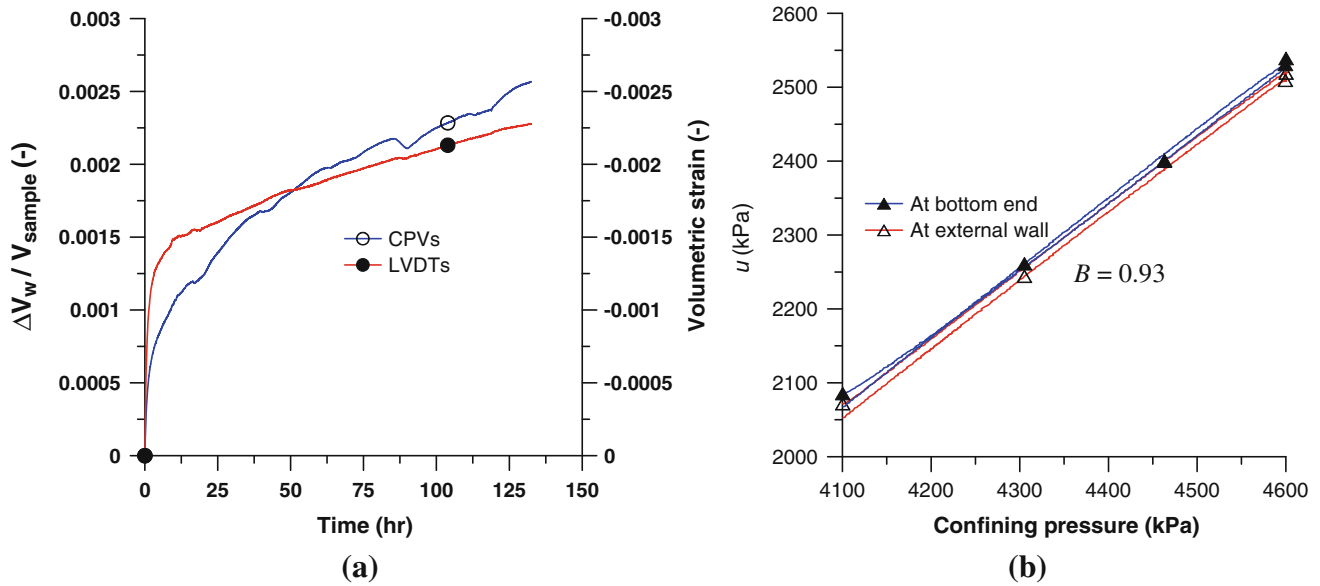


Fig. 4 **a** Water intake by sample during resaturation phase (injected by CPVs) and sample volumetric response by the local strain transducers (LVDTs), **b** undrained isotropic compression test at the

end of the resaturation phase to measure the Skempton coefficient, induced pore pressure in the sample in function of confining pressure

enhanced lateral ones) should be kept open and the temperature elevation should be slow enough in order to avoid important excess thermal pore pressure inside the sample. This heating rate can be numerically estimated by solving the pore pressure diffusion equation with appropriate sample parameters and boundary conditions.

4.1.1 Heating Rate

A numerical analysis is performed to estimate the induced excess pore pressure in sample TO1 when the temperature is increased at a constant rate while keeping the total stress constant ($\Delta p = 0$). In an axisymmetric configuration, adapted to the cylindrical shape of the sample and considering the possible anisotropy of the permeability in axial and radial directions, the pore pressure change can be obtained from the following equation (Ghabezloo et al. 2009):

$$\frac{du}{dt} = \Lambda \frac{dT}{dt} + \frac{1}{\mu_w S} \left(k_r \frac{\partial^2 u}{\partial r^2} + k_r \frac{1}{r} \frac{\partial u}{\partial r} + k_z \frac{\partial^2 u}{\partial z^2} \right) \quad (24)$$

where k_r and k_z are the radial and axial permeabilities. The radial and axial permeability values obtained from a transient permeability test run in the hollow cylinder apparatus (Monfared 2011) are equal to 2.5×10^{-20} and $7.5 \times 10^{-20} \text{ m}^2$, respectively. The measured thermal pressurization coefficient is taken equal to 61 kPa/°C (see Sect. 4.2.1), an average value for temperatures between 25 and 80°C. The storage coefficient (S) is obtained from Eq. 10 with the parameters given in Sect. 3.5, giving $S = 1.91 \times 10^{-6} \text{ kPa}^{-1}$. The water compressibility (c_w)

does not change significantly between 25 and 80°C and an average value of $4.43 \times 10^{-7} \text{ kPa}^{-1}$ is adopted. The decrease in water viscosity with temperature is fitted from Spang (2002) data with the following function:

$$\mu_w = 1.865 \times 10^{-7} T^2 - 3.023 \times 10^{-5} T + 1.576 \times 10^{-3} \quad (25)$$

where water viscosity (μ_w) is in Pa s and temperature (T) is in degree centigrade.

The initial and boundary conditions adopted are presented in Fig. 5. The height of the lateral drainages is equal to 30 mm.

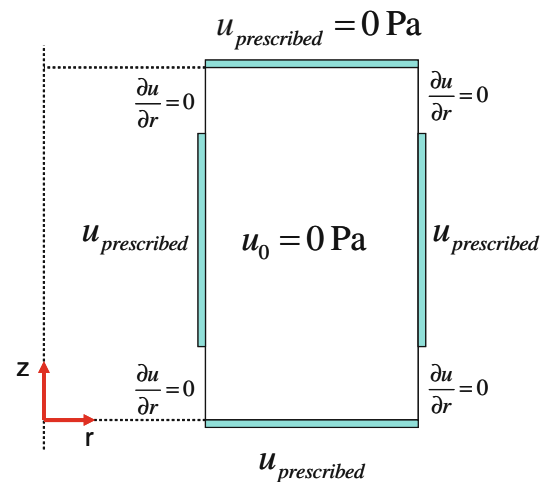


Fig. 5 Optimization of the heating rate: initial and boundary conditions for the numerical simulation of drained heating

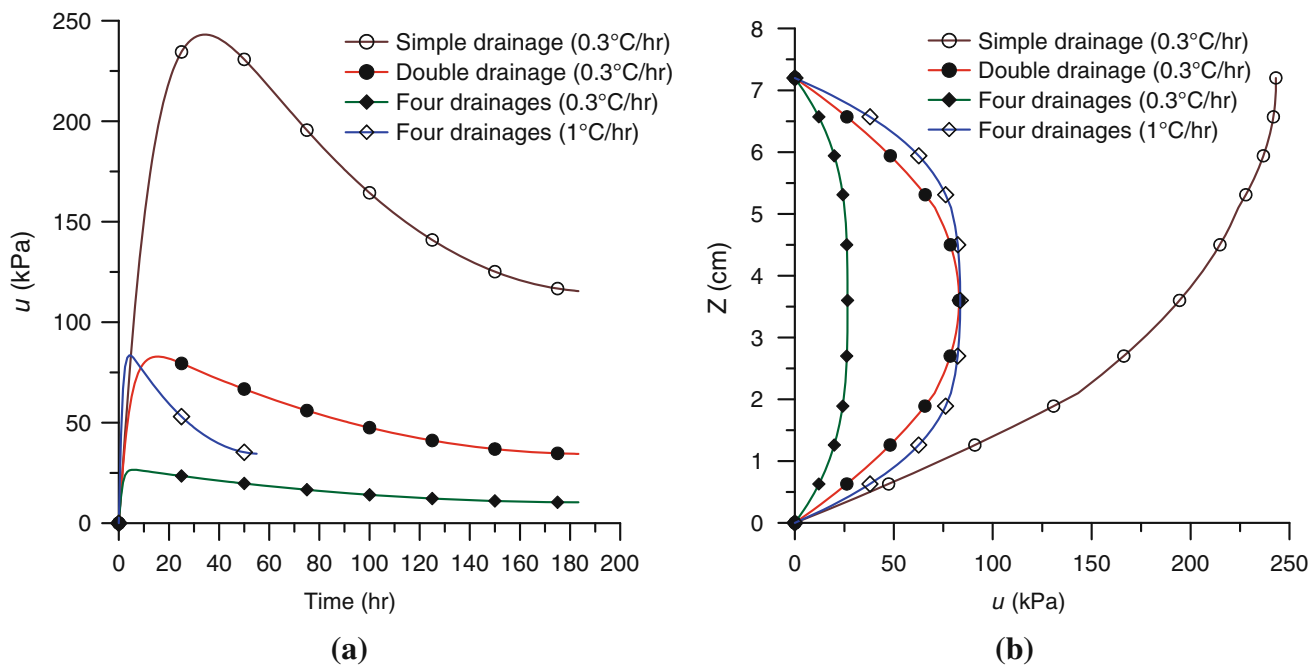


Fig. 6 Numerical analysis of induced pore pressure in the sample during a heating test for different drainage conditions: **a** the induced pore pressure as a function of time for different drainage conditions,

b the profile of pore pressure in half of the thickness of the sample at peak pore pressure

Equation 24 is solved numerically by using a fourth order Runge–Kutta finite differences scheme (see Monfared et al. 2011a for further details on the numerical resolution). First, a heating rate ($\frac{dT}{dt}$) of 0.3°C/h, commonly used to perform drained heating tests in low permeability clayey material in standard triaxial cells (Sultan et al. 2000), was applied. Figure 6a shows the change of pore pressure inside the sample at the point situated at mid-height and mid-thickness as a function of time for the case of standard drainage (at one end and at both ends) and enhanced lateral drainage. All curves in Fig. 6a show a maximum for the induced pore pressure. This maximum can be explained by the competing effect of the source term (thermal pressurization) and the diffusion term (Eq. 24). The source term is dominant before the peak of pressure whereas the diffusion term is dominant after. Figure 6b shows the maximum calculated thermal pore pressure profile during heating from 25 to 80°C along the sample height in half the thickness of the sample under various drainage conditions (at one end, at both ends and with enhanced lateral drainages).

The results show that the maximum induced pore pressure is equal to 243 kPa with drainage at one end (simple drainage). The value decreases to 83 kPa with drainage at both ends (double drainage) and to 27 kPa when lateral drainages enhanced (four drainages). In the two latter cases the induced pore pressure can be considered as negligible (considering the sample compressibility presented in Sect.

3.5). Numerical calculations hence show that a satisfactory drained condition can be achieved by using a heating rate of 0.3°C/h with drainage at both ends. This heating rate can be increased in the hollow cylinder triaxial cell thanks to the enhanced lateral drainages. Figure 6a and b show that with a heating rate of 1°C/h, the excess pore pressure is only 84 kPa which is negligible value as explained above. This heating rate is thus chosen to perform the drained heating test.

4.1.2 Test Results

Two heating–cooling cycles are performed on sample TO1. The volumetric response of the sample during this test is monitored by the response of the LVDT. This direct measurement differs from the indirect evaluation of volume change from the water volume expelled from the sample (Campanella and Mitchell 1968; Baldi et al. 1988), which is strongly dependent on the nature of water (free or adsorbed) and also can be altered by microleaks at high temperature. However, only the radial LVDTs can be used because they are in direct contact with the sample whereas the axial ones are fixed on a supporting ring around the sample and the measured axial strains are altered by the deformation of the supporting ring during heating. The volumetric deformation of the sample is calculated by assuming isotropic thermal expansion of the sample ($\varepsilon_V = 3\varepsilon_{rad}$) and the response is presented in Fig. 7.

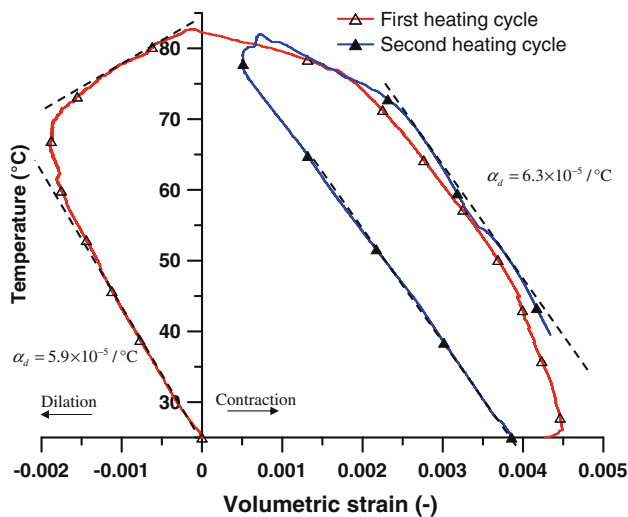


Fig. 7 Drained heating test on Opalinus claystone: volumetric response by the local strain transducers (LVDT type) assuming isotropic response of the sample during thermal loading

It should be noted that the anisotropy of the linear thermal expansion coefficient of the Opalinus claystone reported in the literature is relatively limited. A ratio of about 1.5 is given by Gens et al. (2007) for the coefficient parallel to the bedding when compared with the one perpendicular to it. This figure shows that an initial quasi-linear expansion phase between 25 and 60°C (rate of $5.9 \times 10^{-5}/^{\circ}\text{C}$) is followed by a transition phase and a contraction that starts at 68°C and becomes significant and linear between 70 and 83°C with a rate of $-1 \times 10^{-4}/^{\circ}\text{C}$. During subsequent cooling, the sample quasi linearly contracts with a rate ($6.3 \times 10^{-5}/^{\circ}\text{C}$) close to that of the first heating expansion phase ($5.9 \times 10^{-5}/^{\circ}\text{C}$). An irreversible contraction of 0.45% is finally obtained after the first cycle. The second temperature cycle exhibits a quasi reversible linear response (with the similar rate as the first cooling phase) with a quasi-linear expansion up to 80°C followed by a parallel contraction curve when temperature is decreased.

4.1.3 Discussion

The linear expansion coefficients of Opalinus claystone obtained by different authors and compiled by Muñoz et al. (2009) is presented in Table 3. Volumetric thermal expansion coefficients are derived under the assumption of material isotropy.

In this table, most values have been obtained by back analysis from numerical simulations of in situ thermal experiments carried out at the Mont-Terri URL, except in the case of Muñoz et al. (2009) that concerned a thermal laboratory experiment carried out in a constant volume instrumented cell (temperature and pore pressure). Note that all these experiments were carried out under unknown

Table 3 Thermal expansion coefficient of Opalinus claystone, volumetric thermal expansion coefficients are obtained assuming material isotropy

	Linear thermal expansion coefficient ($^{\circ}\text{C}^{-1}$)	Volumetric thermal expansion coefficient ($^{\circ}\text{C}^{-1}$)
Hohner and Bossart (1998)	1.35×10^{-5}	4.05×10^{-5}
Wileveau (2005)	2.6×10^{-5}	7.8×10^{-5}
Gens et al. (2007)	1.4×10^{-5}	4.2×10^{-5}
Jobman and Polster (2007)	1.5×10^{-5}	4.5×10^{-5}
Muñoz et al. (2009)	1.2×10^{-5}	3.6×10^{-5}

stress conditions. The state of stress applied during the test to the formation (that could not be measured) in the points in which the thermal parameters were deduced depends upon the thermo-mechanical processes involved during the in situ heating tests. They depend on the geometrical 3D configuration of the experiments (complex in the case of in situ tests), on the heating rates and on the thermo-mechanical deformation of the saturated rock (that involves the compressibility and thermal dilation coefficients of water, of the solid grains, together with the drained rock compressibility). In this regard, the parameters directly estimated from test on sample TO1 come from a well-controlled homogeneous situation. Both values obtained from this test (5.9×10^{-5} and $6.3 \times 10^{-5}/^{\circ}\text{C}$) are comparable with the values of the Table 3, although somewhat higher. The good compatibility between these measurements confirms that the first expansion between 25 and 60°C and that the volume changes during the second heating-cooling phase are fully drained and of a thermo-elastic nature.

The subsequent thermal irreversible contraction is comparable to that observed in normally consolidated plastic clays (Baldi et al. 1988; Delage et al. 2000 on Boom clay). In fine-grained soils, this phenomenon is understood as a thermal consolidation of the sample, which corresponds to the rearrangement of the grains after a critical temperature. It seems that the claystone has kept the memory of its maximum supported temperature like overconsolidated soils conserve the memory of the maximum supported load. The sample once heated up to 83°C after the first cycle, keeps expanding up to 80°C (the new maximum temperature supported) during the second cycle, forgetting the previous temperature threshold of 65°C. It is interesting to relate this first temperature threshold to the maximum temperature previously experienced by Opalinus clay. From geological arguments, the maximum burial depth of the Opalinus Clay at Mont Terri is 1,350 m (Tim Vietor, personal communication). Assuming a geothermal gradient of about $0.03^{\circ}\text{C}/\text{m}$, the value of 65°C appears as a plausible maximum temperature experienced by the

material before our test. The observed behavior is typical of thermal hardening, with an elastic thermal expansion observed below the maximum supported temperature, followed by a plastic contraction at yielding once the maximum temperature is attained. Note that the concept of thermal yield has been described in the model developed by Cui et al. (2000) for normally and overconsolidated soils through the mobilization of a specific TY yield curve coupled to a loading yield curve similar to that developed by Hueckel and Borsetto (1990). This approach could certainly be adapted to claystone by accounting for the strong post-sedimentation diagenetic links that characterizes claystones.

The elasto-plastic dilation coefficient (α_d^{ep}) of the sample can be estimated by considering the volumetric response of the sample between 68 and 83°C during the first heating phase, which gives a value of $-1 \times 10^{-4}/^\circ\text{C}$. Thus, the plastic thermal expansion coefficient of Opalinus claystone is obtained from (Sulem et al. 2007):

$$\alpha_d^p = \alpha_d^{ep} - \alpha_d \quad (26)$$

which gives a value of $-1.61 \times 10^{-4}/^\circ\text{C}$. The obtained plastic thermal dilation coefficient for Opalinus claystone is smaller than that for Boom clay ($-7 \times 10^{-4}/^\circ\text{C}$, after Delage et al. 2000) and clayey gouge from Aigion fault ($-3.8 \times 10^{-4}/^\circ\text{C}$, after Sulem et al. 2007), which confirms again the important role of post-sedimentation diagenetic link for this claystone as compared to plastic clays.

4.2 Undrained Thermal Heating

4.2.1 Test Results

The undrained behavior of the Opalinus claystone is investigated on sample TO2 that has been heated from 25 to 55°C in undrained condition starting from an initial stress state close to in situ conditions (confining pressure and back pressure equal to 4.1 and 2.2 MPa, respectively). The same heating rate as in the drained test (1°C/h) has been used so as to ensure pore pressure homogeneity inside the sample (see Sect. 4.1.1). The responses of pore pressure transducers at the bottom and at the external wall of the sample are presented in Fig. 8. This figure shows that the responses of both pressure transducers are similar, which confirms the good homogeneity of the pore pressure field in the sample.

To account for the effects of the drainage system, the measured thermal pressurization coefficient ($\frac{\Delta u}{\Delta T}$) is estimated from the slope of the pore pressure change at each point. The value is then corrected by applying Eq. 19 and the corrected pore pressure change values are obtained from the corrected thermal pressurization coefficient

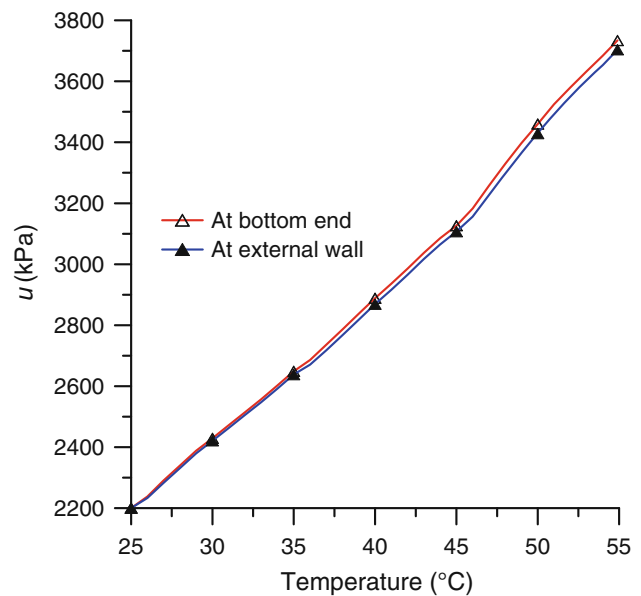


Fig. 8 Undrained heating test on Opalinus claystone sample: Induced pore pressure as a function of temperature

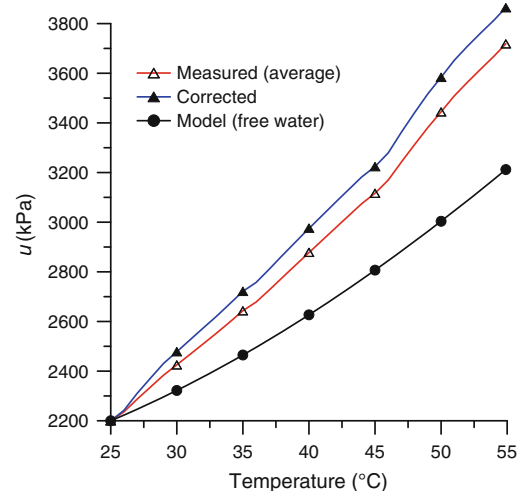


Fig. 9 Correction of the pore pressure measurement by taking into account the effect of the drainage system and calculated induced pore pressure by considering the free water thermal expansion

evaluated at each step ($u_{r_{i+1}} = u_{r_i} + \Lambda_{i+1}^{cor}(T_{i+1} - T_i)$). This curve is plotted in Fig. 9. The sample volume change during this test is measured by the LVDTs and is plotted in Fig. 10. This response must also be corrected to account for the effect of the drainage system as suggested by Eq. 21. The procedure previously used for the pressure curve is used for the volumetric strain curve and the corrected curve is also plotted in Fig. 10.

The thermal pressurization coefficient (Λ) and the undrained thermal expansion coefficient (α_u) of the Opalinus claystone are obtained from the slopes of the corrected

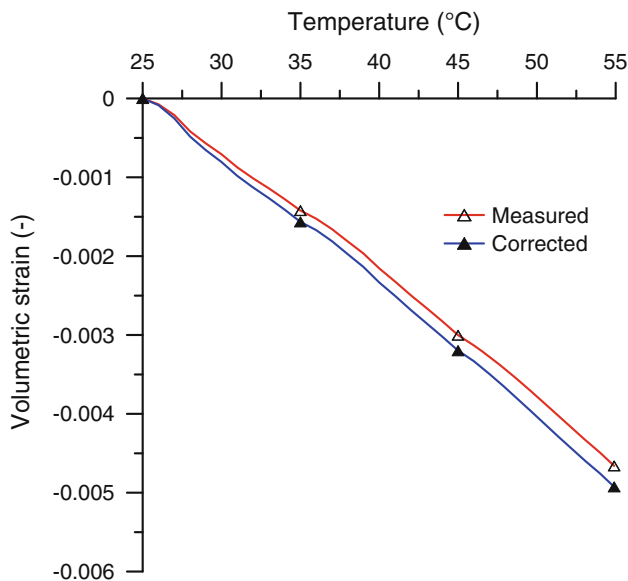


Fig. 10 Volumetric response of the sample during the undrained heating test and corrected data by considering the effect of the drainage system

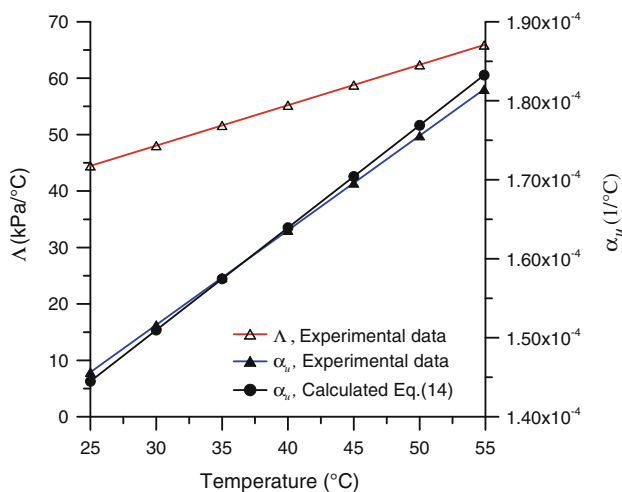


Fig. 11 Thermal pressurization (Δ) and undrained thermal expansion (α_u) coefficient of Opalinus claystone

curves presented in Figs. 9 and 10 respectively, after fitting the curves with a second order polynomial (Fig. 11). The figure shows that the thermal pressurization coefficient increases from 44.5 to 65.9 kPa/°C and the undrained thermal expansion coefficient increases from 1.46×10^{-4} to 1.81×10^{-4} /°C.

4.2.2 Discussion

The experimental results show an increase of the undrained thermal expansion coefficient with temperature. Considering Eq. 14, this increase can be attributed to the increase of the thermal pressurization coefficient with temperature.

Note that the drained compressibility (c_d) does not change with temperature as shown in Campanella and Mitchell (1968) and the solid phase compressibility (c_s) is also assumed to be constant. By considering a value of 1.85×10^{-6} kPa $^{-1}$ for the drained compressibility and using the obtained experimental value for thermal pressurization coefficient, the undrained thermal expansion coefficient (Eq. 14) can be evaluated. As shown in Fig. 11, the experimental values and the theoretical ones are compatible. The compatibility of the theoretical and experimental values confirms the validity of the thermo-poro-elasticity assumption within the applied temperature range. Note that the maximum temperature in this test (55°C) is below 65°C, which is seen as the threshold between thermo-elastic and thermo-plastic response.

The increase of the thermal pressurization coefficient (Δ) with temperature can be linked to the increase of the thermal expansion of water (α_w) with temperature (Eq. 12). The induced pore pressure in the sample is first evaluated by considering the thermal expansion of pore water as the one of free pure water. Figure 9 clearly shows that by considering the thermal expansion of free pure water the evaluated induced pressure is lower than the measured one. Thus, in order to reproduce the experimental data the pore water thermal expansion should be higher than free pure water. Baldi et al. (1988) have shown that the experimental results of thermal tests on low porosity clays could not be modeled by considering the free water thermal expansion coefficient. These authors proposed to explain this difference by considering a double layer model and assuming that the water layer in the vicinity of clay plate is under a higher pressure than that of free water. They showed that below 40°C, the thermal expansion of water in low porosity clay is higher than that of free water but the rate of increase of the thermal expansion with temperature in these materials is lower. Another possible reason for the higher thermal expansion coefficient of water in materials with small pores is given by Xu et al. (2004). These authors show that the water when confined in the nanopores of porous silica glasses has a higher thermal expansion coefficient compared to that of free water. Based on experimental results, a higher thermal expansion coefficient of the pore water in cementitious materials is also evidenced by Valenza and Scherer (2005) and Ghabezloo et al. (2009). It is shown that this anomaly of the thermal behavior of water confined in nanopores is significant when the pore size is smaller than 15 nm (Valenza and Scherer 2005). Regarding the pore size distribution of Opalinus claystone (Muñoz 2006), around 50% of the pores have a diameter smaller than 15 nm. Thus, this important fraction of small pore size is probably the main reason of the higher thermal expansion coefficient of the Opalinus claystone pore water. We note that also the Opalinus claystone water

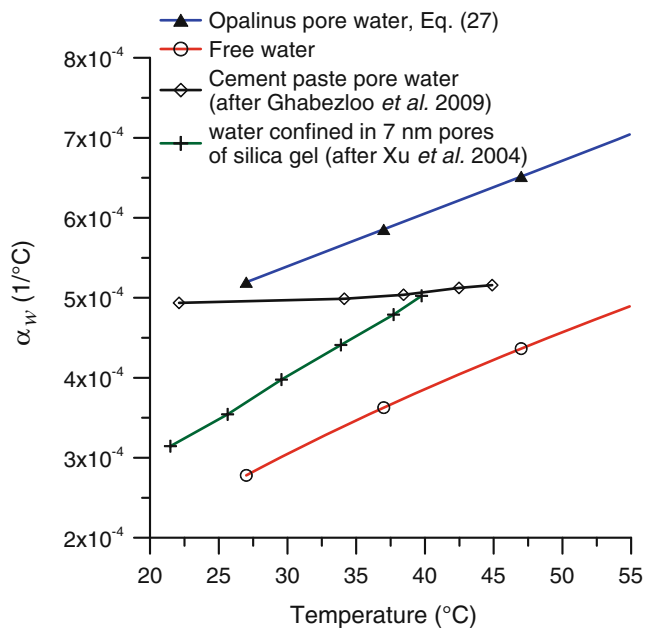


Fig. 12 Estimation of the thermal expansion coefficient of Opalinus claystone pore water and comparison with the existing data in the literature

is of marine origin and the concentration of the ions such Na^+ (0.169 mol/l) and Cl^- (0.16 mol/l) is important in this water (Pearson et al. 2003). The presence of ions can also increase the thermal expansion of water as discussed by Ghabezloo et al. (2009).

The thermal expansion of Opalinus claystone water can be back analyzed from the results of the undrained tests by using the following relation:

$$\alpha_w = \alpha_s + \frac{\alpha_u - \alpha_d}{\phi B} \quad (27)$$

The thermal dilation of the solid phase can be estimated as an average of the thermal dilation of the minerals which gives a value of $3 \times 10^{-5}/^\circ\text{C}$. The Skempton coefficient is taken equal to 0.95 (see Sect. 3.5). Figure 12 shows the estimated thermal expansion coefficient of Opalinus claystone water from Eq. 27 and that of free water as well as the thermal expansion of cement paste pore water (Ghabezloo et al. 2009) and pore water confined in 7 nm pores of silica gel (Xu et al. 2004). The estimated thermal expansion of Opalinus pore water is relatively higher than the others, which is probably related to the important fraction of nano pores in this claystone. The increasing rate of the thermal expansion of Opalinus pore water is slightly lower than that of free water.

5 Conclusion

In this study, the thermal properties of saturated Opalinus claystone in drained and undrained condition have been

investigated through laboratory tests performed in a new triaxial cell with short drainage path (10 mm). Two samples of Opalinus claystone have been resaturated under an isotropic stress state equivalent to the effective in situ one in order to minimize swelling and induced damage during the resaturation phase. Two drained heating–cooling cycles have been performed with a slow rate of $1^\circ\text{C}/\text{h}$ and it is shown through a numerical analysis that this rate is sufficiently slow to ensure negligible excess pore water pressure in the sample. The volumetric response of the sample during the first cycle presents a thermo-elasto-plastic response with sample dilation up to 65°C followed by sample contraction up to 83°C . During the cooling phase of the first cycle and also the second heating–cooling cycle, a quasi elastic behavior of the sample has been observed, which confirms thermal hardening of the sample. Interestingly, the temperature threshold of 65°C is a plausible value for the maximum temperature previously experienced by Opalinus claystone during geological burial up to 1,350 m.

The undrained behavior of the sample is investigated on the second sample. It was shown that the temperature increase in undrained condition induces an excess pore pressure in the sample. The similarity of the responses of both pressure transducers proves the homogeneity of the pressure in the sample. The obtained thermal pressurization coefficient and undrained thermal expansion coefficient are compatible regarding a thermo-poro-elasticity framework. The induced pore pressure in the sample cannot be modeled by the thermal expansion of free pure water and the back analysis of the test results show a higher thermal expansion coefficient for pore water in Opalinus claystone.

Acknowledgments The authors wish to acknowledge the financial support provided by the European project TIMODAZ (F16W-CT-2007-036449 coordinated by EURIDICE, Dr. Li Xiang-Ling) and by NAGRA for this research. Dr. T Vietor, from NAGRA, is also acknowledged for providing the samples of Opalinus claystone and for fruitful discussions. They also wish to thank the technical team of Navier/CERMES (Ecole des ponts ParisTech) for its assistance in the experimental work and Prof. Y.J. Cui and Dr. S. Ghabezloo for stimulating discussions.

References

- ANDRA. Dossier (2005) Référentiel du site Meuse/Haute Marne. Tome 2; Report CRPADS040022_B
- Baldi G, Hueckel T, Pellegrini R (1988) Thermal volume changes of the mineral-water system in low-porosity clay soils. *Can Geotech J* 25:807–825
- Bastiaens W, Bernier F, Li XL (2007) SELFRAC: experiments and conclusions on fracturing, self-healing and self-sealing processes in clays. *J Phys Chem Earth* 32:600–615
- Bishop AW (1976) Influence of system compressibility on observed pore pressure response to an undrained change in stress in saturated rock. *Géotechnique* 26(2):371–375

- Bossart P, Meier PM, Moeri A, Trick T, Mayor JC (2002) Geological and hydraulic characterisation of the excavation disturbed zone in the Opalinus claystone of the Mont-Terri Rock Laboratory. *Eng Geol* 66:19–38
- Campanella RG, Mitchell JK (1968) Influence of temperature variations on soil behavior. *J Soil Mech Found Div Proc Am Soc Civil Eng* 94(SM3):709–734
- Coussy O (2004) *Poromechanics*. Wiley, Chichester
- Cui YJ, Sultan N, Delage P (2000) A thermomechanical model for saturated clays. *Can Geotech J* 37:607–620
- Delage P, Le TT, Tang AM, Cui YJ, Li XL (2007) Suction effects in deep Boom clays samples. *Géotechnique* 57(2):239–244
- Delage P, Sultan N, Cui YJ (2000) On the thermal consolidation of boom clay. *Can Geotech J* 37:343–354
- Ghabezloo S, Sulem J, Saint-Marc J (2009) The effect of undrained heating on a hardened cement paste. *Cem Concr Res* 39(1):54–64
- Ghabezloo S, Sulem J (2010) Effect of the volume of the drainage system on the measurement of undrained thermo-poro-elastic parameters. *Int J Rock Mech Min Sci* 47:60–68
- Gens A, Vaunat J, Garitte B, Wileveau Y (2007) In situ behavior of a stiff layered clay subject to thermal loading: observations and interpretation. *Géotechnique* 57(2):207–228
- Hohner M, Bossart P (1998) Geological, mineralogical, geochemical, geomechanical and hydraulic parameters of Opalinus Clay derived by in-situ and laboratory experiments, Mont Terri Technical Note 98–49. Geotechnical Institute Ltd, Berne
- Hueckel T, Borsetto M (1990) Thermoplasticity of saturated soils and shales: constitutive equations. *J Geotech Eng* 116(1):1765–1777
- Hueckel T, Pellegrini R (1991) Thermoplastic modeling of undrained failure of saturated clay due to heating. *Soils Found* 31(3):1–16
- Jobmann M, Polster M (2007) The response of Opalinus claystone due to heating: a combined analysis of in situ measurement, laboratory investigations and numerical calculations. *Phys Chem Earth* 32(8–14):929–936
- Kull H, Jockwer N, Zhang CL, Wileveau Y, Pepa S (2007) Measurement of thermally-induced pore-water pressure increase and gas migration in the Opalinus Clay at Mont Terri. *Phys Chem Earth* 32:937–946
- Martin CD, Lanyon GW (2003) Measurement of in-situ stress in weak rocks at Mont Terri Rock Laboratory, Switzerland. *Int J Rock Mech Min Sci* 40(7–8):1077–1088
- Mazurek M (1999) Mineralogy of the Opalinus clay. In: Thury M, Bossart, P (eds) Results of the hydrogeological, geochemical and geotechnical experiments, performed in 1996 and 1997. Swiss National Geological and Hydrogeological Survey, Geological Report, vol 23, pp 15–18
- McTigue DF (1986) Thermoelastic response of fluid-saturated porous rock. *J Geophys Res* 91(B9):9533–9542
- Mohajerani M, Delage P, Monfared M, Sulem J, Tang AM, Gatmiri B (2011) Oedometric compression and swelling behavior of the Callovo-Oxfordian argillite. *Int J Rock Mech Min Sci* 48(4):606–615
- Monfared M, Delage P, Sulem J, Mohajerani M, Tang AM, De Laure E (2011a) A new hollow cylinder triaxial cell to study the behavior of geomaterials with low permeability. *Int J Rock Mech Min Sci* 48(4):637–649
- Monfared M, Sulem J, Delage P, Mohajerani M (2011b) Reactivation of a shear band by thermal pressurization of pore water in a saturated clay. *J Eng Geol* (submitted)
- Monfared M (2011) *Couplages température-endommagement-perméabilité dans les sols et les roches argileux*. PhD thesis, Université Paris-Est, Ecole des Ponts ParisTech, p 210
- Mügler C, Filippi M, Montarnal Ph, Martinez JM, Wileveau Y (2006) Determination of the thermal conductivity of Opalinus claystone via simulations of experiments performed at the Mont Terri underground laboratory. *J Appl Geophys* 25:112–129
- Muñoz JJ (2006) Thermo-hydro-mechanical analysis of soft rock application to a large scale heating test and large scale ventilation test. PhD thesis, University Politecnica de Catalunya, p 246
- Muñoz JJ, Alonso EE, Lloret A (2009) Thermo-hydraulic characterisation of soft rock by means of heating pulse tests. *Géotechnique* 59(4):293–306
- Nagra (2002b) Calculations of the temperature evolution of a repository for spent fuel, vitrified high-level waste and intermediate level waste in opalinus claystone. Nagra Technischer Bericht NTB 01-04, p 28
- Pearson FJ, Arcos D, Bath A, Boisson JY, Fernandez AM, Gäbler HE, Gaucher E, Gautschi A, Griffault L, Hernan P, Waber HN (2003). Mont Terri Project-geochemistry of water in the Opalinus claystone formation at the Mont Terri rock laboratory. Reports of the FOWG, Geology Series-N°5
- Rice JR (2006) Heating and weakening of faults during earthquake slip. *J Geophys Res* 111:B05311
- Spang B (2002) Excel add-in for properties of water and steam in SI-units. <http://www.cheresources.com/iapwsif97.shtml>
- Sulem J, Lazar P, Vardoulakis I (2007) Thermo-poro-mechanical properties of clayey gouge and application to rapid fault shearing. *Int J Numer Anal Methods Geomech* 31(3):523–540
- Sultan N, Delage P, Cui YJ (2000) Comportement thermomécanique de l'argile de Boom. *Comptes Rendus de l'Académie des Sciences, Series IIB. Mechanics* 328(6):457–463
- Thury M, Bossart P (1999) The Mont Terri rock laboratory, a new international research project in a Mesozoic shale formation, in Switzerland. *Eng Geol* 52:347–359
- Valenza JJ, Scherer GW (2005) Evidence of anomalous thermal expansion of water in cement paste. *Cem Concr Res* 35:57–66
- Wileveau Y (2005) THM behavior of host rock (HE-D) experiment: progress report. Part 1, Technical Report TR 2005-03. Mont Terri Project
- Xu S, Simmons GC, Scherer GW (2004) Thermal expansion and viscosity of confined liquids. *Mat. Res. Soc. Symp. Proc.*, vol 790, Materials Res. Soc, Warrendale: P6.8.1–P6.8.7
- Zhang CL, Rothfuchs T, Su K, Hoteit N (2007) Experimental study of the thermo-hydro-mechanical behavior of indurated clays. *Phys Chem Earth* 32(8–14):957–965